

To appear in *The Astrophysical Journal*

Scattering by Interstellar Dust Grains. I. Optical and Ultraviolet

B.T. Draine

Princeton University Observatory, Peyton Hall, Princeton, NJ 08544;
draine@astro.princeton.edu

ABSTRACT

Scattering and absorption properties at optical and ultraviolet wavelengths are calculated for an interstellar dust model consisting of carbonaceous grains and amorphous silicate grains. Polarization as a function of scattering angle is calculated for selected wavelengths from the infrared to the vacuum ultraviolet.

The widely-used Henyey-Greenstein phase function provides a good approximation for the scattering phase function at wavelengths between ~ 0.4 and $1\mu\text{m}$, but fails to fit the calculated phase functions at shorter and longer wavelengths. A new analytic phase function is presented. It is exact at long wavelengths, and provides a good fit to the numerically-calculated phase function for $\lambda > 0.27\mu\text{m}$.

Observational determinations of the scattering albedo and $\langle \cos \theta \rangle$ show considerable disagreement, especially in the ultraviolet. Possible reasons for this are discussed.

Subject headings: dust, extinction – polarization – scattering – ultraviolet: ISM

1. Introduction

Interstellar grains scatter electromagnetic radiation. Reflection nebulosities are conspicuous at optical and UV wavelengths when dust is brightly illuminated by a nearby star. Dust clouds which are not unusually close to a star are illuminated by the general interstellar radiation field. Finally, the starlight scattered by dust in the diffuse interstellar medium constitutes the so-called “diffuse galactic light”. Observations of reflection nebulae, dust clouds, and the diffuse galactic light, provide a means of determining the scattering properties of interstellar grains, thereby testing models for interstellar dust.

Photoionization and photodissociation of molecules play a major role in interstellar chemistry, and the chemical structure of molecular clouds is therefore directly linked to the ability of ultraviolet starlight to penetrate into these dusty regions. Knowledge of dust scattering properties in the ultraviolet is therefore required for realistic modeling of interstellar clouds.

The nature of interstellar grains remains uncertain (see Draine 2003a, and references therein). This paper will examine the scattering properties for a grain model consisting of two separate grain

populations – carbonaceous grains and silicate grains. With the grains approximated by homogeneous spheres with the size distributions found by Weingartner & Draine (2001; hereafter WD01), this grain model is consistent with the observed interstellar extinction, the observed infrared emission from interstellar dust (Li & Draine 2001, 2002), and the X-ray scattering halo observed around Nova Cygni 1992 (Draine & Tan 2003). The carbonaceous grains are assumed to be primarily carbon when the grains are large, but to extend down to very small sizes with the smallest grains being individual polycyclic aromatic hydrocarbon molecules. The scattering is dominated by grains with radii $a \gtrsim 100 \text{ \AA}$, containing $\gtrsim 10^6$ atoms; carbonaceous grains in this size range are modeled using the optical properties of graphite.

The primary objective of this paper is to calculate the scattering and extinction properties of this dust model at infrared, optical, and ultraviolet wavelengths, and to make these results available for use in radiative transfer calculations and for comparison with observations. The X-ray scattering and absorption properties of this grain model are the subject of Paper II (Draine 2003b).

The adopted dielectric functions are presented in §2. The scattering properties of interstellar dust at optical and ultraviolet energies, as calculated for the carbonaceous-silicate grain model, are presented in §3. We show the scattering phase function at selected wavelengths from the SDSS z band ($\lambda = 8930 \text{ \AA}$) to the vacuum ultraviolet ($\lambda = 1820 \text{ \AA}$). Scattering properties are calculated for Milky Way dust with $R_V = 3.1$, and also for models for dust in the LMC and SMC. In §3.2 we show the degree of polarization as a function of scattering angle for selected wavelengths.

The Henyey-Greenstein phase function has often been used to approximate the anisotropic scattering properties of interstellar dust. In §4.1 we show that the Henyey-Greenstein function has r.m.s. error $< 10\%$ for $0.47 \mu\text{m} < \lambda < 0.94 \mu\text{m}$, but has larger errors outside this range. We present a new analytic phase function (equation 5) with a wider range of applicability, with r.m.s. error $< 10\%$ for $\lambda > 0.27 \mu\text{m}$.

In §5 we collect observational determinations of the scattering albedo and $\langle \cos \theta \rangle$ for dust in reflection nebulae, in dense clouds, and in the diffuse interstellar medium. Discrepancies among these determinations are noted, and possible reasons for this are discussed.

The principal results are summarized in §6

2. Dielectric Function

As discussed by WD01, the grain population is assumed to include very small grains with the optical properties of polycyclic aromatic hydrocarbon molecules (PAHs), plus larger grains which are approximated as carbonaceous or silicate spheres. The PAHs produce negligible scattering.

From the observed $3.4 \mu\text{m}$ C-H stretch feature, Pendleton & Allamandola (2002) estimate that $\sim 85\%$ of the C is aromatic, and $\sim 15\%$ is aliphatic (chainlike). The graphite dielectric function will be used to approximate the optical and ultraviolet response of interstellar carbonaceous grain

material. Scattering and absorption by the carbonaceous spheres is calculated using the dielectric tensor of graphite, using the usual “1/3-2/3 approximation” (Draine & Malhotra 1993).

The dielectric functions used here are taken from Paper II, which constructs self-consistent dielectric functions extending from microwave to X-ray energies, including realistic structure near X-ray absorption edges. The adopted dielectric functions for graphite and “astronomical silicate” are shown in Figures 1 and 2. These dielectric functions are close to the dielectric functions obtained previously by Draine & Lee (1984), although differing in detail.

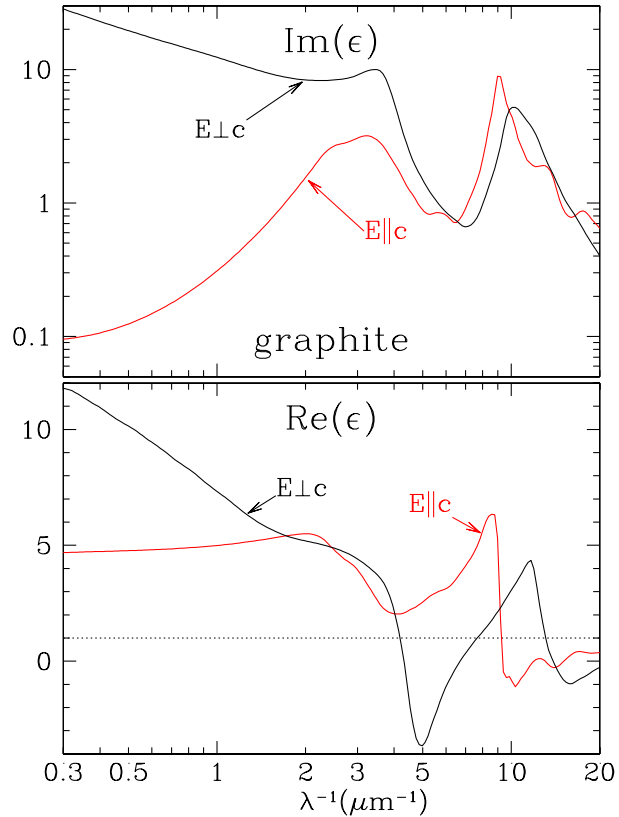


Fig. 1.— Dielectric function for graphite (Draine 2003b).

3. IR-Optical-UV Scattering by Interstellar Dust

3.1. Angular Distribution of Scattered Light

Weingartner & Draine (2001; hereafter WD01) obtained size distributions of spherical carbonaceous and silicate grains which reproduce the observed extinction curve both in the local Milky Way and in the Large and Small Magellanic Clouds. Here we calculate the scattering properties of these dust mixtures.

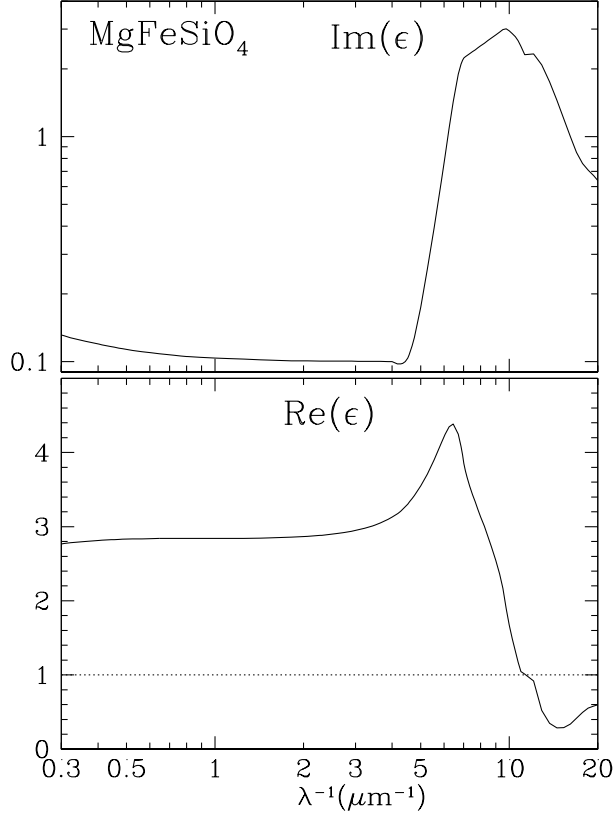


Fig. 2.— Dielectric function adopted for amorphous MgFeSiO_4 (Draine 2003b).

The scattering properties of a particular dust mixture X are characterized by the differential scattering cross section per H nucleon

$$\left(\frac{d\sigma_{\text{sca}}(\lambda, \theta)}{d\Omega} \right)_X = \sum_j \int da \left(\frac{1}{n_{\text{H}}} \frac{dn_j}{da} \right)_X \left(\frac{dC_{\text{sca}}}{d\Omega} \right)_{j,a,\lambda} , \quad (1)$$

where $n_{\text{H}}^{-1}(dn_j/da)da$ is the number of grains of type j per H nucleon with radii in $(a, a + da)$, and $(dC_{\text{sca}}/d\Omega)_{j,a,\lambda}$ is the differential scattering cross section for grain type j , radius a , at wavelength λ , for scattering angle θ , for a grain illuminated by unpolarized light. The grains are assumed to be spherical, and the differential scattering cross sections are calculated using Mie theory (Bohren & Huffman 1984), using the code developed by Wiscombe (1980, 1996).

In Figure 3 we show the differential scattering cross section per H nucleon for $R_V = 3.1$ Milky Way dust, at the central wavelengths of SDSS z (8930Å), i (7480Å), r (6165Å), g (4685Å), and u (3550Å), Cousins I (8020Å) and R (6492Å), V (5470Å), and the F250W (2696Å), F220W (2220Å), and F25CN182 (1820Å) filters for the Space Telescope Imaging Spectrograph (STIS). The scattering becomes stronger and more forward-throwing at shorter wavelengths.

To see the sensitivity to variations in the dust mixture, Fig. 3 also shows $d\sigma_{\text{sca}}/d\Omega$ calculated

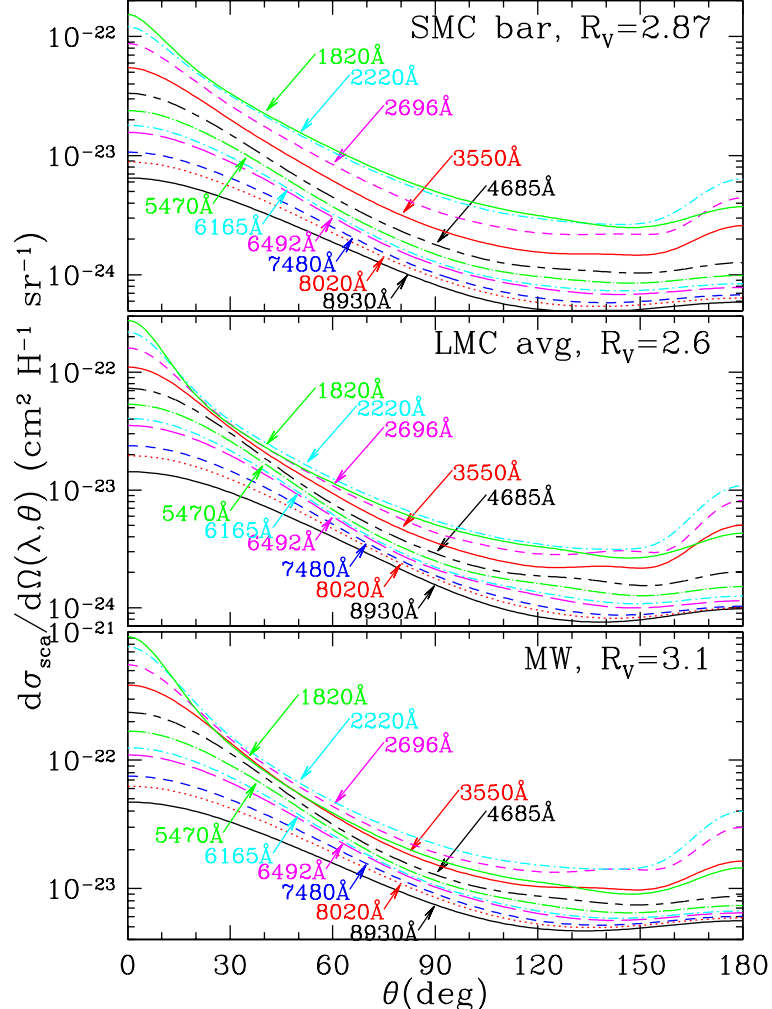


Fig. 3.— $d\sigma_{\text{sca}}/d\Omega$ at selected wavelengths λ , as a function of the scattering angle θ , for WD01 models for Milky Way dust with $R_V = 3.1$, LMC average dust, and SMC bar dust. Curves are labelled by wavelength λ .

for the WD01 dust mixtures for the “average LMC” and the SMC bar. The calculated scattering closely resembles the Milky Way scattering, but with an overall reduction of about a factor of 4 for the LMC, and a factor of 8 for the SMC, in line with the overall dust and metal abundance relative to the Milky Way.¹

Figure 4 shows the wavelength dependence of σ_{ext} (the total extinction cross section per H), the scattering albedo $\sigma_{\text{sca}}/\sigma_{\text{ext}}$, and the first and second moments² $\langle \cos \theta \rangle$ and $\langle \cos^2 \theta \rangle$ for the

¹Ne/H is $\sim 30\%$ of solar in the LMC and $\sim 14\%$ of solar in the SMC (Dufour 1984; Kurt & Dufour 1998). In the LMC, $E(B - V)/N_{\text{H}}$ is $\sim 24\%$ of the local Milky Way value (Koornneef 1982; Fitzpatrick 1986) while in the SMC it is only $\sim 13\%$ of the local value (Martin et al. 1989).

²The second moment $\langle \cos^2 \rangle$ will be used in the new analytic phase function proposed in §4.2.

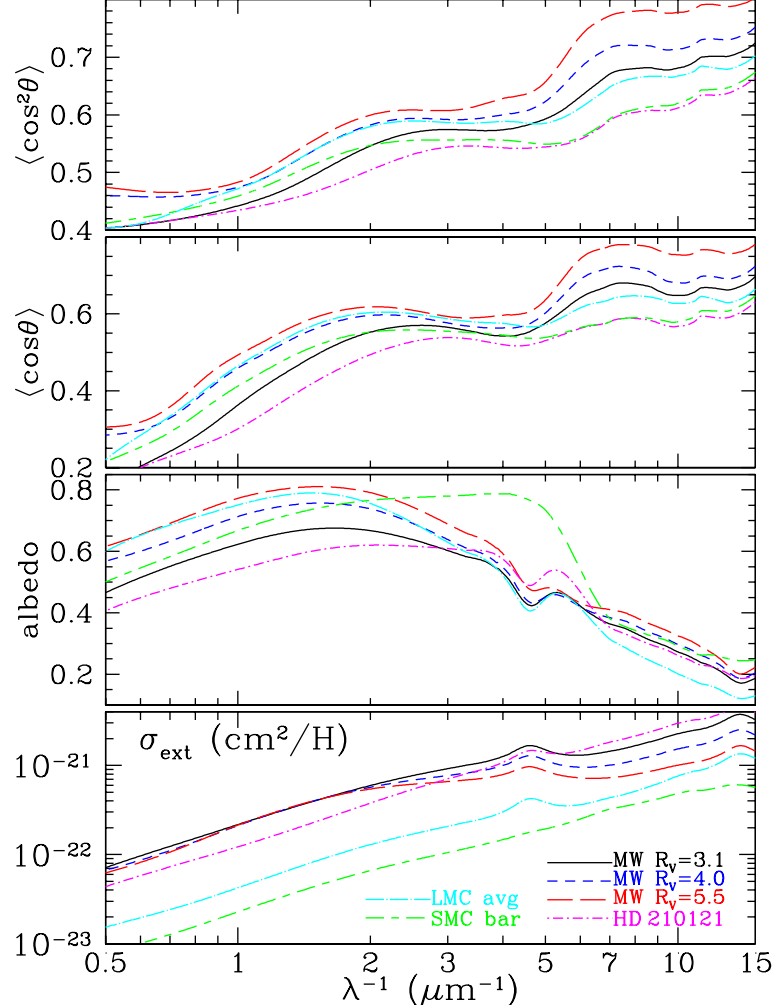


Fig. 4.— Extinction cross section per H, albedo, $\langle \cos \rangle$, and $\langle \cos^2 \rangle$ calculated for WD01 models for Milky Way dust with $R_V = 3.1$, 4.0, and 5.5, average LMC dust, and dust in the SMC bar.

scattered radiation. Six different grain models are shown, fitted to different observed extinction curves (see WD01 for details). There are considerable differences in albedo, $\langle \cos \rangle$, and $\langle \cos^2 \rangle$ among the models. In particular, the SMC bar model shows a high albedo near $4.6\mu\text{m}^{-1}$, in contrast to the other five models which have a local minimum in the albedo at this frequency. This is because the SMC bar model differs from the other 5 models in lacking PAHs and $a \lesssim 0.02\mu\text{m}$ graphite grains, as these are not allowed by the observed absence of a $4.6\mu\text{m}^{-1}$ extinction “bump”.

3.2. Polarization of Scattered Light

Even when a grain is illuminated by unpolarized light, the scattered radiation is generally polarized. The degree of polarization depends upon both the scattering angle and the wavelength of the radiation. The fractional polarization $P \equiv (I_{\perp} - I_{\parallel})/(I_{\perp} + I_{\parallel})$, where I_{\perp}, I_{\parallel} are the intensities of scattered light in polarization modes perpendicular or parallel to the scattering plane.

The polarization P of the scattered light is shown in Fig. 5 as a function of scattering angle θ for Milky Way dust with $R_V = 3.1$, at 11 different wavelengths. Rayleigh scattering would have $P = (1 - \cos^2 \theta)/(1 + \cos^2 \theta)$, with $P = 1$ for $\theta = 90^\circ$. At long wavelengths, the polarization has a distinct peak near $\sim 90^\circ$, but even for $\lambda \approx 0.9\mu\text{m}$ the peak polarization is only ~ 0.45 . As the wavelength is reduced, the peak polarization declines. For $\lambda \lesssim 0.6\mu\text{m}$, the polarization becomes negative at large scattering angles (see Figure 5), with large negative polarizations in the $120\text{--}150^\circ$ region for $0.2\mu\text{m} \lesssim \lambda \lesssim 0.4\mu\text{m}$. Note, however, that this negative polarization occurs for scattering angles where the scattering is very weak (see Figure 3) and therefore could be masked by scattering at other points on the sightline where the scattering contributes a positive polarization. Observations of the predicted negative polarization will probably require simple scattering geometries, such as dust in a thin disk, illuminated by a single source.

Similar results are found for the LMC and SMC dust mixtures – see Fig. 5. Note the very large negative polarizations found for the LMC mixture for $0.2\mu\text{m} \lesssim \lambda \lesssim 0.55\mu\text{m}$. From the variation of the ultraviolet polarization signature between the different grain size distributions in Figure 5 it is apparent that the ultraviolet polarization is sensitive to the details of the grain size distribution.

4. Analytic Approximations for the Phase Function

4.1. Henyey-Greenstein Phase Function

Scattering of unpolarized incident light by a dust mixture at wavelength λ is characterized by the total scattering cross section per H nucleon, $\sigma_{\text{sca}}(\lambda)$, and a “phase function”

$$\Phi(\theta, \lambda) \equiv \frac{1}{\sigma_{\text{sca}}(\lambda)} \frac{d\sigma_{\text{sca}}(\theta, \lambda)}{d\Omega} \quad (2)$$

characterizing the angular distribution of the scattered light, where $d\sigma_{\text{sca}}/d\Omega$ is the differential scattering cross section, at scattering angle θ , for unpolarized incident light. The definition (2) implies the normalization $\int d\Omega \Phi = 1$. Isotropic scattering would have $\Phi = 1/4\pi$. The first moment

$$\langle \cos \theta \rangle = \int d\Omega \cos \theta \Phi(\theta, \lambda) \quad (3)$$

of the phase function is a measure of the asymmetry between forward and backward scattering.

Henyey & Greenstein (1941) proposed an analytic function to model anisotropic scattering for

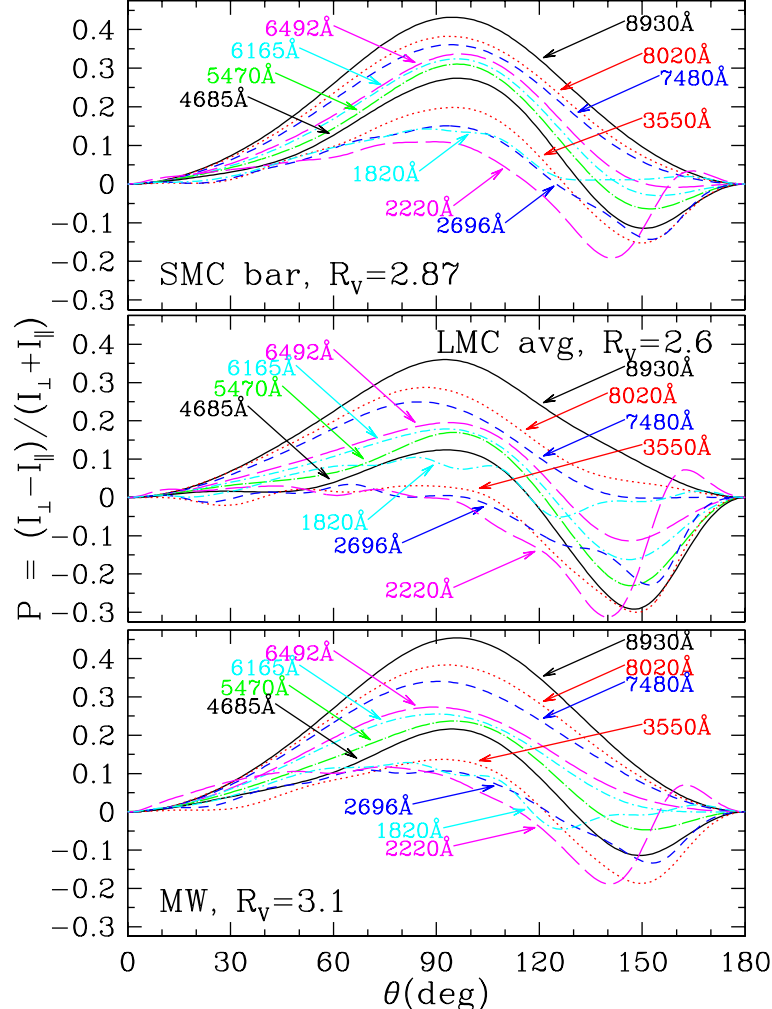


Fig. 5.— Degree of polarization as a function of scattering angle θ , for scattering by Milky Way dust with $R_V = 3.1$, LMC average dust, and SMC bar dust. Curves are labelled by wavelength λ .

dust grain mixtures:

$$\phi_0(\theta) = \frac{1}{4\pi} \frac{1 - g^2}{(1 + g^2 - 2g \cos \theta)^{3/2}} \quad , \quad g = \langle \cos \theta \rangle \quad . \quad (4)$$

With a single parameter g , this is a convenient analytic form that has been widely used to represent dust scattering properties in radiative models of dusty regions.

By construction, $\phi_0(\theta)$ has the correct first moment $\langle \cos \theta \rangle = \int d\Omega \cos \theta \phi_0(\theta) = g$, but of course ϕ_0 does not perfectly reproduce the angular dependence of the real phase function $\Phi(\theta)$. As will be seen below, ϕ_0 is a poor approximation at both $\lambda \lesssim 0.4\mu\text{m}$ and $\lambda > 1\mu\text{m}$.

4.2. A New Phase Function

At long wavelengths, Rayleigh scattering prevails, with $\langle \cos \theta \rangle \rightarrow 0$ and $\Phi \rightarrow (3/16\pi)(1 + \cos^2 \theta)$. When $\langle \cos \theta \rangle \rightarrow 0$, the Henyey-Greenstein phase function $\phi_0 \rightarrow 1/4\pi$; ϕ_0 is 33% low at $\theta = 0, \pi$ and 33% high at $\theta = \pi/2$.

Consider the phase function

$$\phi_\alpha(\theta) = \frac{1}{4\pi} \left[\frac{1 - g^2}{1 + \alpha(1 + 2g^2)/3} \right] \frac{1 + \alpha \cos^2 \theta}{(1 + g^2 - 2g \cos \theta)^{3/2}} , \quad (5)$$

with two adjustable parameters, α and g . For $\alpha = 0$, equation (5) reduces to the Henyey-Greenstein phase function ϕ_0 (equation 4). For $g = 0$ and $\alpha = 1$ this reduces to the phase function for Rayleigh scattering. For $\alpha = 1$ this corresponds to the phase function proposed by Cornette & Shanks (1992). Analytic results for this phase function are given in Appendices A - C.

To determine the parameters α and g we can require that $\phi_\alpha(\theta)$ have the same first and second moments $\langle \cos \theta \rangle$ and $\langle \cos^2 \theta \rangle$ as Φ . The parameters g and α are then given by equations (B4-B6). However, although the resulting phase function has correct first and second moments, the fit is poor when the dust is strongly forward-scattering ($\langle \cos \theta \rangle \gtrsim 0.6$).

We find that an improved fit is obtained if we obtain g and α from equations (B4-B6) only when the resulting $\alpha \leq 1$; for values of $\langle \cos \theta \rangle$ and $\langle \cos^2 \theta \rangle$ for which equations (B4-B6) lead to $\alpha > 1$, we instead set $\alpha = 1$ and obtain g from equation (C2). We will refer to this new analytic phase function as $\phi_{\alpha \leq 1}$.

Figure 6 shows the scattering phase function $\Phi(\theta)$ for the WD01 Milky Way dust model, together with the Henyey-Greenstein phase function ϕ_0 and our new phase function $\phi_{\alpha \leq 1}$, at wavelengths $\lambda = 1.2\mu\text{m}$, $0.80\mu\text{m}$, and $0.40\mu\text{m}$. For these three wavelengths, the new phase function provides an improved fit to the actual phase function Φ . For $\lambda = 0.40\mu\text{m}$, we also show Φ approximated by a sum over Legendre polynomials P_l up to $l = 8$. This 9 term expansion does not reproduce Φ as well as the new phase function $\phi_{\alpha \leq 1}$.

At ultraviolet wavelengths the grains become more forward-throwing, and the analytic phase functions ϕ_0 and $\phi_{\alpha \leq 1}$ no longer provide a good fit, as seen in Figure 7 for $\lambda = 0.20\mu\text{m}$ and $0.10\mu\text{m}$. At $\lambda = 0.20\mu\text{m}$, for example, both the Henyey-Greenstein phase function ϕ_0 and the new phase function $\phi_{\alpha \leq 1}$ underestimate the forward scattering intensity by a factor of ~ 2 for $\cos \theta \gtrsim 0.98$ ($\theta \lesssim 10^\circ$).

To quantify the error associated with using an analytic phase function $\phi(\theta)$ to approximate an actual phase function $\Phi(\theta)$, we define the r.m.s. relative error

$$h_{\text{rel}} \equiv \left[\int \frac{d\Omega}{4\pi} \left[\frac{\phi(\theta) - \Phi(\theta)}{\Phi(\theta)} \right]^2 \right]^{1/2} , \quad (6)$$

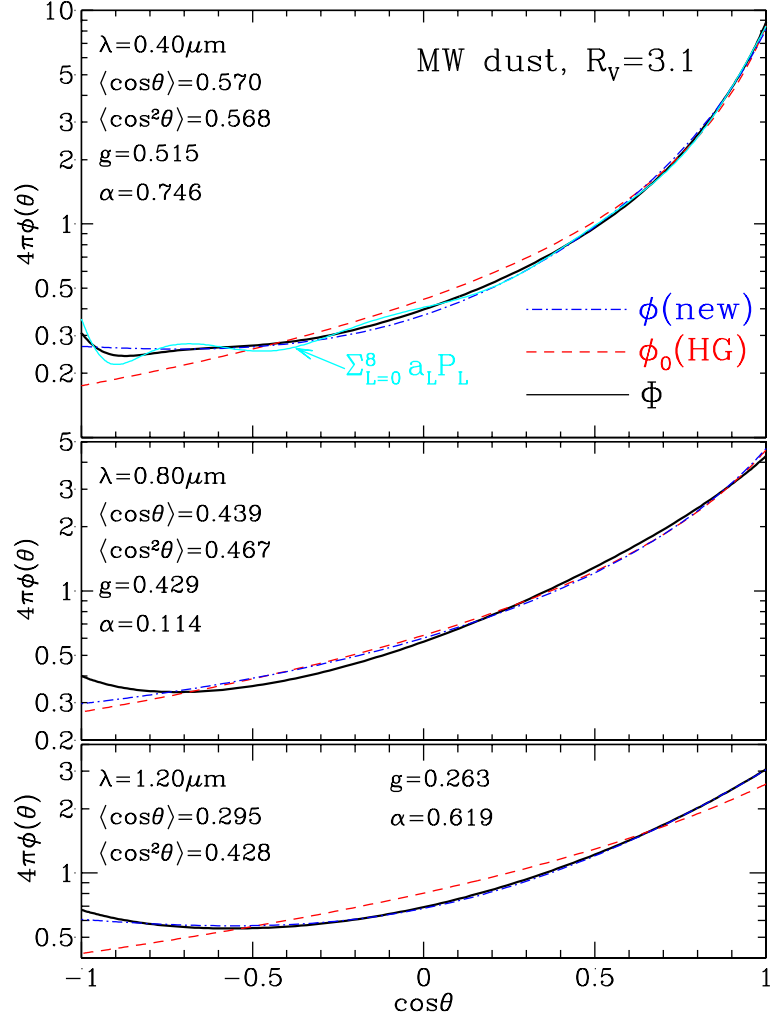


Fig. 6.— Scattering phase function for the WD01 Milky Way dust model at three wavelengths (solid lines) compared to the Henyey-Greenstein phase function ϕ_0 and our new phase function $\phi_{\alpha \leq 1}$. For $\lambda = 0.4\mu\text{m}$ a 9 term Legendre polynomial representation is also shown.

and r.m.s. absolute error

$$h_{\text{abs}} \equiv \left[\int \frac{d\Omega}{4\pi} \left[\frac{\phi(\theta) - \Phi(\theta)}{\langle \Phi \rangle} \right]^2 \right]^{1/2} . \quad (7)$$

where, of course, $\langle \Phi \rangle = 1/4\pi$. The r.m.s. relative error h_{rel} would appear to be the best measure of the overall quality of fit. h_{rel} and h_{abs} will differ substantially only when the phase function is very asymmetric; large fractional errors in directions where the scattering is weak then make only a small contribution to h_{abs} , while modest fractional errors in directions where the scattering is very strong will make large contributions to h_{abs} .

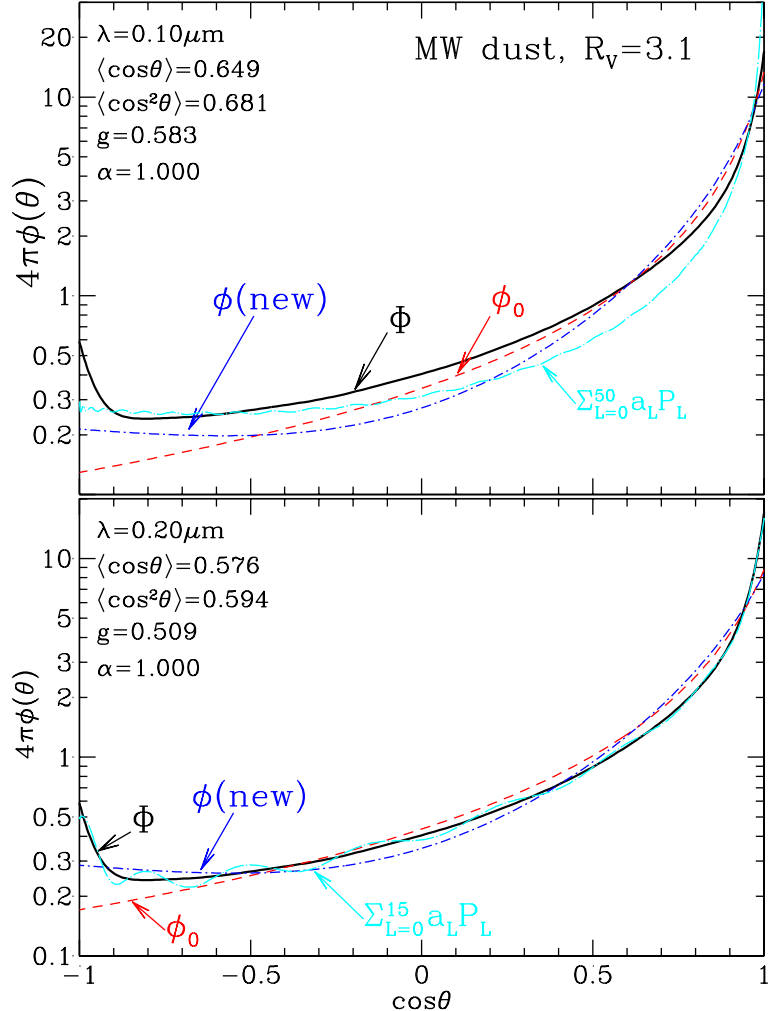


Fig. 7.— Same as Figure 6, but for $\lambda = 0.2\mu\text{m}$ and $0.1\mu\text{m}$. Legendre polynomial representations of $\Phi(\theta)$ are shown with 16 and 51 terms.

In the limit of Rayleigh scattering ($\lambda \gg a$), $\Phi(\theta) \rightarrow \frac{3}{4}(1 + \cos^2\theta)$, and ϕ_0 has errors

$$h_{\text{abs}} \rightarrow 1/\sqrt{20} \approx 0.22 \quad , \quad (8)$$

$$h_{\text{rel}} \rightarrow (13 - 4\pi)^{1/2}/3 \approx 0.22 \quad . \quad (9)$$

Figure 8 compares the error of different analytic approximations to the phase function, using as an example $\Phi(\theta, \lambda)$ for the WD01 model for $R_V = 3.1$ Milky Way dust. The errors h_{rel} and h_{abs} are shown in Figure 8 for the Henyey-Greenstein function ϕ_0 , the Cornette-Shanks phase function ϕ_1 , and our new phase function $\phi_{\alpha \leq 1}$. At long wavelengths $\lambda \gtrsim 3\mu\text{m}$, the Henyey-Greenstein approximation ϕ_0 has $h_{\text{rel}} \approx h_{\text{abs}} \approx 0.22$, as expected from eq. (8,9). Between ~ 0.5 and $\sim 1\mu\text{m}$, the relative errors for ϕ_0 are modest, $h_{\text{rel}} < 10\%$, so ϕ_0 provides a good approximation to the actual scattering properties. However, ϕ_0 has $h_{\text{rel}} > 10\%$ for $\lambda < 0.5\mu\text{m}$, rising to shorter wavelengths.

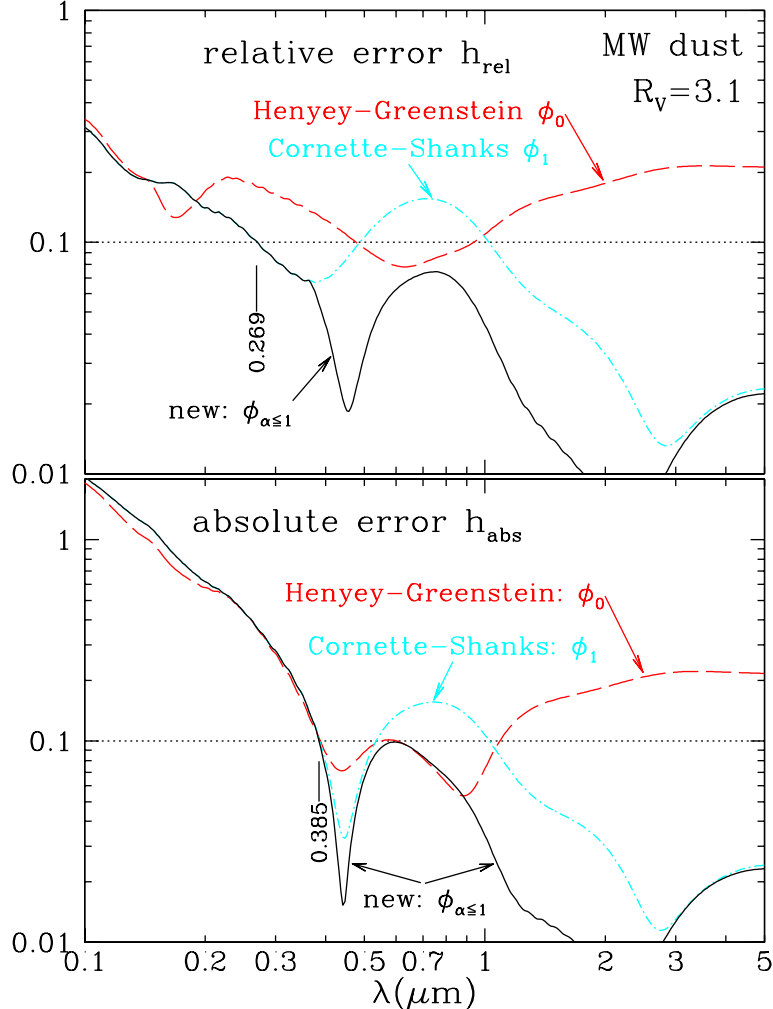


Fig. 8.— Normalized relative error h_{rel} (eq. 6) and absolute error h_{abs} (eq. 7) for the analytic phase functions ϕ_0 , ϕ_1 , and $\phi_{\alpha \leq 1}$ applied to the WD01 grain model for MW dust with $R_V = 3.1$.

Figure 8 shows the fractional errors h_{rel} and h_{abs} for the new phase function $\phi_{\alpha \leq 1}$. As expected, the new phase function provides an excellent fit at long wavelengths, with fractional errors $< 3\%$ for $\lambda > 1\mu\text{m}$. As the wavelength is decreased, the new phase function $\phi_{\alpha \leq 1}$ (as measured by h_{rel}) remains preferable to the Henyey-Greenstein phase function for $\lambda \gtrsim 0.19\mu\text{m}$. $\phi_{\alpha \leq 1}$ has $h_{\text{rel}} < 10\%$ for $\lambda > 0.27\mu\text{m}$.

In the ultraviolet the phase function becomes very strongly forward-scattering, and all of the the analytic approximations have significant errors. More complicated parameterizations – such as the use of multiple Henyey-Greenstein phase functions, as by Witt (1977) and Hong (1985) – may be considered. Alternatively, a given phase function $\Phi(\theta)$ can be approximated by summing over Legendre polynomials, although the sum needs to include a large number of terms to provide a good approximation – 16 terms are required for $\lambda = 0.20\mu\text{m}$, and even 51 terms are insufficient

for $\lambda = 0.10\mu\text{m}$. At short wavelengths it may be best to simply tabulate $\Phi(\theta)$ and interpolate as required.

5. Discussion

The scattering properties of interstellar dust have been determined observationally by comparing the observed surface brightness of reflection nebulae with model nebulae computed with different dust scattering properties, selecting the model which provides the best match to the observations. The usual approach has been to try to determine only two grain properties – the albedo and $\langle \cos \theta \rangle$ – by finding radiative transfer models which appear to be consistent with the observed surface brightness of scattered light.

It has been customary to assume that the scattering phase function $\Phi(\theta)$ can be approximated by the Henyey-Greenstein function $\phi_0(\theta)$, with $g = \langle \cos \theta \rangle$

This approach has been used with (1) observations of high surface brightness reflection nebulae (e.g., NGC 2023, NGC 7023, IC 435) illuminated primarily by a single star, (2) observations of individual dust clouds illuminated by ambient starlight, and (3) observations of the much fainter diffuse galactic light (the entire Galaxy as a reflection nebulosity). Figures 9 and 10 show the results so obtained from a number of independent studies, at wavelengths from the optical to vacuum ultraviolet. Also shown are the albedo and asymmetry factor calculated for WD01 grain models representing average Milky Way dust with $R_V \equiv A_V/E(B-V) = 3.1$, and dust from denser regions with $R_V = 4.0$ and 5.5 . While there are differences among the different observational determinations, particularly in the ultraviolet, many of the observational results are in general agreement with the albedo and asymmetry factor calculated for the WD01 grain model.

For $\lambda^{-1} < 4\mu\text{m}^{-1}$, the observational studies appear to be in general agreement with one another, but at shorter wavelengths the observational results are sometimes in conflict. For example, from observations of the diffuse galactic light at $\sim 6.25\mu\text{m}^{-1}$ ($\lambda = 0.16\mu\text{m}$) Hurwitz et al. (1991) found $(a, g) = (0.185 \pm 0.055, 0.2 \pm 0.2)$, while Witt et al. (1997) found $(a, g) = (0.45 \pm 0.05, 0.68 \pm 0.10)$.

Aside from genuine regional variations in dust properties, there are many factors which could contribute to such discrepancies. Foremost may simply be the difficulty of observations in the vacuum ultraviolet, followed by uncertainties concerning the nebular geometry and the illuminating radiation. However, given that use of the Henyey-Greenstein phase function ϕ_0 introduces an absolute error $h_{\text{abs}} \gtrsim 70\%$ in the scattering phase function at $\lambda < 0.16\mu\text{m}$ (see Fig. 8), it seems possible that reliance on the Henyey-Greenstein phase function may contribute to the disagreements among different observational determinations of the albedo and scattering asymmetry in the ultraviolet.

Unfortunately, the new phase function $\phi_{\alpha \leq 1}$ is inaccurate for $\lambda < 0.27\mu\text{m}$. For $\lambda^{-1} \gtrsim 4\mu\text{m}^{-1}$, radiative transfer models should use a more accurate representation of the phase function Φ . As discussed above, one possibility is expansion in Legendre polynomials, although many terms are

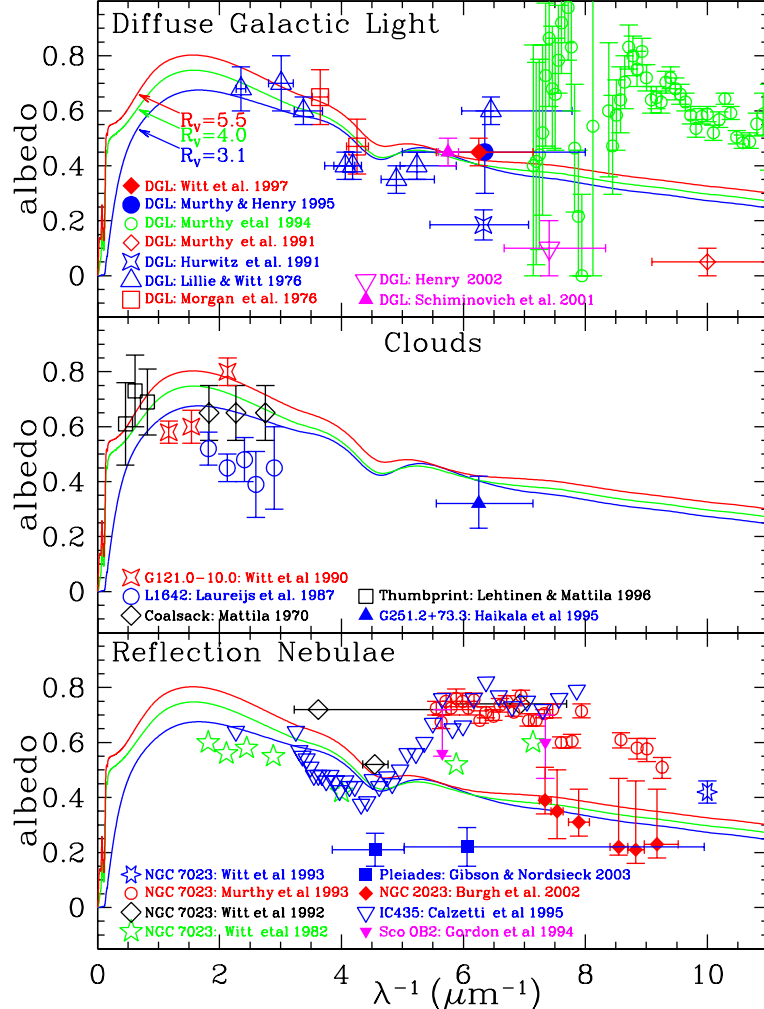


Fig. 9.— Scattering albedo as a function of frequency for different MW dust mixtures, together with observational estimates of the dust albedo in various regions.

required. Alternatively, it may be simplest to use tabulated values of Φ with interpolation. “Inversion” of the observational data to infer the grain properties may not be feasible; the best approach may be to assume the dust properties [i.e., $\sigma_{\text{ext}}(\lambda)$, albedo(λ), and $\Phi(\theta, \lambda)$] based on a grain model, and then seek a dust spatial distribution which maximizes consistency with the observed surface brightness and whatever other constraints are available. Failure to find agreement would suggest that the grain model may be incorrect.

Applying this approach to reflection nebulae is complicated by the possibility of clumpy dust distributions, which Mathis et al. (2002) show can produce a range of ratios of nebular surface brightness to unscattered stellar flux, depending on the detailed dust clump distribution and the viewing direction. Diffuse clouds (i.e., the diffuse galactic light) and externally-illuminated clouds may prove easier to interpret than bright reflection nebulae, which generally have a bright star

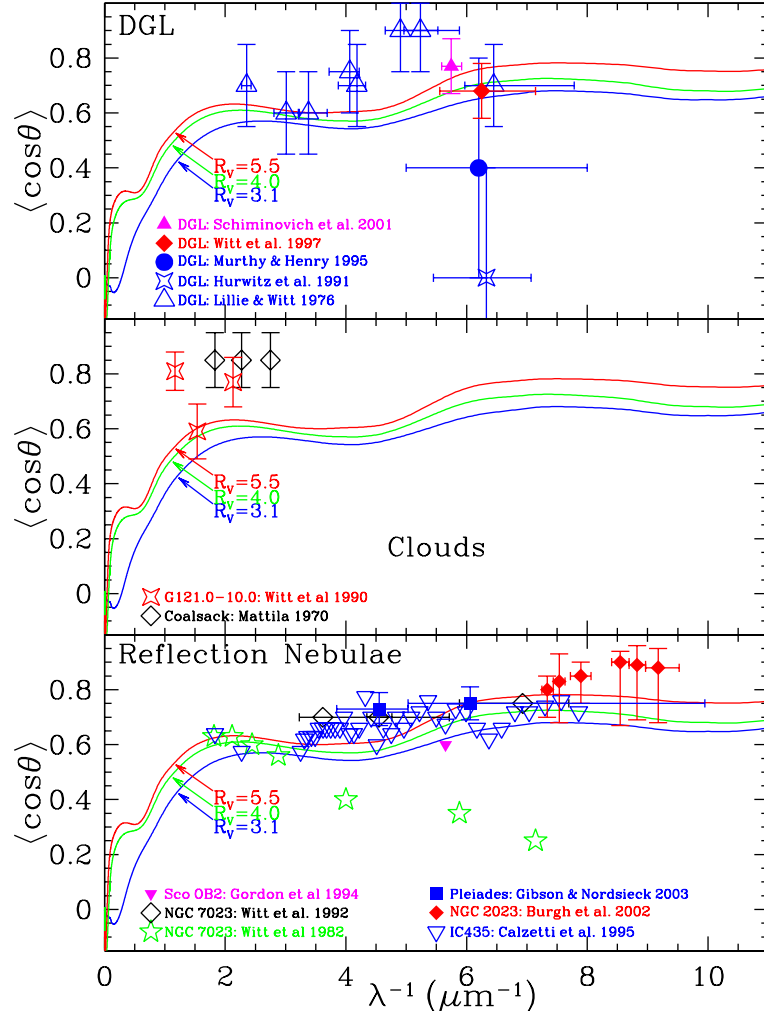


Fig. 10.— Scattering asymmetry factor $g = \langle \cos \theta \rangle$ as a function of frequency for different MW dust mixtures. Also shown are observational estimates for g in various regions.

embedded in the dust distribution.

6. Summary

The following are the principal results of this work:

1. Differential scattering cross sections have been calculated at selected wavelengths from infrared to ultraviolet for dust mixtures appropriate to the diffuse interstellar medium in the Milky Way, the LMC, and the SMC. These scattering functions, which can be used for modeling reflection nebulae, are available at <http://www.astro.princeton.edu/~draine> .

2. The polarization of scattered light, as a function of scattering angle, is calculated at selected wavelengths.
3. The calculated phase function $\Phi(\theta)$ for the WD01 model for $R_V = 3.1$ MW dust is compared to the widely-used Henyey-Greenstein phase function $\phi_0(\theta)$. At wavelengths $0.48\mu\text{m} < \lambda < 0.96\mu\text{m}$, ϕ_0 provides a good fit to Φ , with r.m.s. relative error $h_{\text{rel}} < 10\%$. In the ultraviolet, however, ϕ_0 provides a poor fit, with r.m.s. absolute error $h_{\text{abs}} > 50\%$ at $\lambda < 2400\text{\AA}$. The Henyey-Greenstein phase function is not suitable for accurate modeling of reflection nebulae in the ultraviolet.
4. A new phase function, $\phi_{\alpha \leq 1}(\theta)$ is proposed [see equation (5)]. This phase function provides a good approximation to our calculated phase functions for $\lambda > 0.27\mu\text{m}$, with r.m.s. relative error $h_{\text{rel}} < 10\%$. At shorter wavelengths, however, Φ becomes strongly forward-throwing, and neither the Henyey-Greenstein phase function ϕ_0 nor the new phase function $\phi_{\alpha \leq 1}$ provide good approximations.
5. There are significant discrepancies among observational determinations of the albedo and $\langle \cos \theta \rangle$ in the ultraviolet for the diffuse galactic light and dust in discrete clouds and reflection nebulae. One possible cause for these discrepancies may be reliance on the Henyey-Greenstein phase function in the radiative transfer models. It is recommended that the new phase function $\phi_{\alpha \leq 1}$ be used at wavelengths $\lambda \gtrsim 0.27\mu\text{m}$; at shorter wavelengths accurate radiative transfer models should use some other procedure to obtain Φ .

I thank Karl Gordon, Aigen Li, Kalevi Mattila, Jonathan Tan, Adolf Witt, and Michael Woolf for valuable comments, the anonymous referee for helpful suggestions, and Robert Lupton for making available the SM software package. This work was supported in part by NSF grant AST-9988126.

A. Phase Function Moments

A phase function of the form

$$\phi_{\alpha}(\theta) = \frac{1}{4\pi} \left[\frac{1 - g^2}{1 + \alpha(1 + 2g^2)/3} \right] \frac{1 + \alpha \cos^2 \theta}{(1 + g^2 - 2g \cos \theta)^{3/2}} \quad (\text{A1})$$

has first and second moments given by

$$\langle \cos \theta \rangle = g \frac{1 + \alpha(3 + 2g^2)/5}{1 + \alpha(1 + 2g^2)/3} , \quad (\text{A2})$$

$$\langle \cos^2 \theta \rangle = \frac{1 + 2g^2 + (3\alpha/35)(7 + 20g^2 + 8g^4)}{3 + \alpha(1 + 2g^2)} . \quad (\text{A3})$$

B. Reproduce $\langle \cos \theta \rangle$ and $\langle \cos^2 \theta \rangle$

If we specify $\langle \cos \theta \rangle$ and $\langle \cos^2 \theta \rangle$, the adjustable parameters g and α are determined from equations (A2,A3). It can be shown that g satisfies the cubic equation

$$g^3 - \frac{17}{3}\langle \cos \theta \rangle g^2 + 7\langle \cos^2 \theta \rangle g - \frac{7}{3}\langle \cos \theta \rangle = 0 \quad . \quad (\text{B1})$$

Let

$$a \equiv \frac{7}{3}\langle \cos^2 \theta \rangle - \frac{289}{81}\langle \cos \theta \rangle^2 \quad , \quad (\text{B2})$$

$$b \equiv \frac{119}{18}\langle \cos \theta \rangle \langle \cos^2 \theta \rangle - \frac{4913}{729}\langle \cos \theta \rangle^3 - \frac{7}{6}\langle \cos \theta \rangle \quad . \quad (\text{B3})$$

If $a^3 + b^2 > 0$, the solution is

$$g = \left[(a^3 + b^2)^{1/2} - b \right]^{1/3} - \left[(a^3 + b^2)^{1/2} + b \right]^{1/3} + \frac{17}{9}\langle \cos \theta \rangle \quad , \quad (\text{B4})$$

whereas if $a^3 + b^2 < 0$, the appropriate root is

$$g = 2|a|^{1/2} \cos(\psi/3) + \frac{17}{9} \cos \theta \quad , \quad \psi \equiv \arccos \left(-b/|a|^{3/2} \right) \quad . \quad (\text{B5})$$

The parameter α is then obtained from equation (A2):

$$\alpha = \frac{25(\langle \cos \theta \rangle - g)}{3(3 + 2g^2)g - 5(1 + 2g^2)\langle \cos \theta \rangle} \quad . \quad (\text{B6})$$

C. Fix α , Reproduce $\langle \cos \theta \rangle$

If we choose to fix the value of α and $\langle \cos \theta \rangle$, then g must satisfy

$$g^3 - \frac{5}{3}\langle \cos \theta \rangle g^2 + \left(\frac{3\alpha + 5}{2\alpha} \right) g - \frac{5}{6\alpha}(3 + \alpha)\langle \cos \theta \rangle = 0 \quad . \quad (\text{C1})$$

For $\alpha \neq 0$, equation (C1) has the real root

$$g = \left[(a_\alpha^3 + b_\alpha^2)^{1/2} + b_\alpha \right]^{1/3} - \left[(a_\alpha^3 + b_\alpha^2)^{1/2} - b_\alpha \right]^{1/3} + \frac{5}{9}\langle \cos \theta \rangle \quad , \quad (\text{C2})$$

$$a_\alpha \equiv \frac{1}{2} + \frac{5}{6\alpha} - \frac{25}{81}\langle \cos \theta \rangle^2 \quad , \quad (\text{C3})$$

$$b_\alpha \equiv \frac{125}{729}\langle \cos \theta \rangle^3 + \frac{5}{9\alpha}\langle \cos \theta \rangle \quad . \quad (\text{C4})$$

For $\alpha \rightarrow 0$ (the Henyey-Greenstein phase function) we see immediately that equation (C1) requires $g = \langle \cos \theta \rangle$.

REFERENCES

Bohren, C.F., & Huffman, D.R. 1983, *Absorption and Scattering of Light by Small Particles* (New York: Wiley)

Burgh, E.B., McCandliss, S.R., & Feldman, P.D. 2002, *ApJ*, 575, 240

Calzetti, D., Bohlin, R.C., Gordon, K.D., Witt, A.N., & Bianchi, L. 1995, *ApJ*, 446, L97

Cornette, W.M., & Shanks, J.G. 1992, *Appl. Optics*, 31, 3152

Draine, B.T. 2003a, *ARA&A*, 41, 241

Draine, B.T. 2003b, *ApJ*, accepted (Paper II) astro-ph/0308251

Draine, B.T., & Lee, H.-M. 1984, *ApJ*, 468, 269 (DL84)

Draine, B.T., & Malhotra, S. 1993, *ApJ*, 414, 632

Draine, B.T., & Tan, J.C. 2003, *ApJ*, 594, 000 (Sept 1) [<http://arxiv.org/abs/astroph/0208302>]

Dufour, R.J. 1984, in IAU Symp. 108, *Structure and Evolution of the Magellanic Clouds*, ed. S. van den Bergh & K.S. de Boer (Dordrecht: Reidel), 353

Fitzpatrick, E.L. 1986, *AJ*, 92, 1068

Gibson, S.J., & Nordsieck, K.H. 2003, *ApJ*, 589, 362

Gordon, K.D., Witt, A.N., Carruthers, G.R., Christensen, S.A., Dohne, B.C. 1994, *ApJ*, 432, 641

Haikala, L.K., Mattila, K., Bowyer, S., Sasseen, T.P., Lampton, M., & Knude, J. 1995, *ApJ*, 443, L33

Henry, R.C. 2002, *ApJ*, 570, 697

Henyey, L.G., & Greenstein, J.L. 1941, *ApJ*, 93, 70

Hong, S.S. 1985, *A&A*, 146, 67

Hurwitz, M., Bowyer, S., & Martin, C. 1991, *ApJ*, 372, 167

Koornneef, J. 1982, *A&A*, 107, 247

Kurt, C.M., & Dufour, R.J. 1998, *Rev. Mex. Astr. Ap.* 7, 202

Laureijs, R.J., Mattila, K., & Schnur, G. 1987, *A&A*, 184, 269

Lehtinen, K., & Mattila, K. 1996, *A&A*, 309, 570

Li, A., & Draine, B.T. 2001, *ApJ*, 554, 778

Li, A., & Draine, B.T. 2002, *ApJ*, 572, 232

Lillie, C.F., & Witt, A.N. 1976, *ApJ*, 208, 64

Martin, N, Maurice, E., & Lequeux, J. 1989, *AA*, 215, 129

Mathis, J.S., Whitney, B.A., & Wood, K. 2002, *ApJ*, 574, 812

Mattila, K. 1970, *A&A*, 9, 53

Morgan, D.H., Nandy, K., & Thompson, G.I. 1976, *MNRAS*, 177, 531

Murthy, J., Dring, A., Henry, R.C., Kruk, J.W., Blair, W.P., Kimble, R.A., & Durrance, S.T. 1993, *ApJ*, 408, L97

Murthy, J., & Henry, R.C. 1995, *ApJ*, 448, 848

Murthy, J., Henry, R.C., & Holberg, J.B. 1991, *ApJ*, 383, 198

Murthy, J., Henry, R.C., & Holberg, J.B. 1994, *ApJ*, 428, 233

Pendleton, Y.J., & Allamandola, L.J. 2002, *ApJS*, 138, 75

Schiminovich, D., Friedman, P.G., Martin, C., & Morrissey, P.F. 2001, *ApJ*, 563, L161

Weingartner, J.C., & Draine, B.T. 2001, *ApJ*, 548, 296 (WD01)

Wiscombe, W.J. 1980, *Appl. Opt.*, 19, 1505

Wiscombe, W.J. 1996, NCAR Technical Note NCAR/TN-140+STR,
ftp://climate.gsfc.nasa.gov/pub/wiscombe/SingleScatt/Homogen_Sphere/Exact_Mie/NCARMieReport.pdf

Witt, A.N. 1977, *ApJS*, 35, 1

Witt, A.N., Friedmann, B.C., & Sasseen, T.P. 1997, *ApJ*, 481, 809

Witt, A.N., Oliveri, M.V., & Schild, R.E. 1990, *AJ*, 99, 888

Witt, A.N., Petersohn, J.K., Bohlin, R.C., O'Connell, R.W., Roberts, M.S., et al., 1992, *ApJ*, 395, L5

Witt, A.N., Petersohn, J.K., Holberg, J.B., Murthy, J., Dring, A., & Henry, R.C. 1993, *ApJ*, 410, 714

Witt, A.N., Walker, G.A.H., Bohlin, R.C., & Stecher, T.P. 1982, *ApJ*, 261, 492